Photocatalytic degradation of 1,2-dichloroethane using immobilized PAni-TiO$_2$ nanocomposite in a pilot-scale packed bed reactor

Mahdi Mohsenzadeh[a], Seyed Ahmad Mirbagheri[a,*], Samad Sabbaghi[b]

[a]Department of Environmental Engineering, Faculty of Civil Engineering, K.N. Toosi University of Technology, Tehran, Iran,
Tel. +989121374357; email: mirbagheri@kntu.ac.ir (S.A. Mirbagheri), Tel. +989177036671; emails: mohsenzadeh@mail.kntu.ac.ir,
mahdi.mohsenzadeh@gmail.com (M. Mohsenzadeh)
[b]Faculty of Advanced Technologies, NanoChemical Engineering Department, Shiraz University, Shiraz, Iran,
Tel. +989171133471; emails: sabbaghi@shirazu.ac.ir, samad.sabbaghi@uwaterloo.ca (S. Sabbaghi)

ABSTRACT

1,2-Dichloroethane is one of the most important chlorinated volatile organic pollutants in wastewaters and has been listed as a priority pollutant by several regulatory organizations worldwide including United States Environmental Protection Agency (EPA). It is widely used as a precursor of the petrochemical industry to produce vinyl chloride monomer for the production of poly vinyl chloride (PVC). In this study, PAni-TiO$_2$ nanocomposite was synthesized by in-situ deposition oxidative polymerization method and its performance for photocatalytic degradation of synthetic 1,2-dichloroethane wastewater was investigated. A new pilot-scale packed-bed continuous photocatalytic reactor was designed and constructed. Glass beads were selected as the packing material. Immobilization was carried out using a modified dip coating and heat attachment method. The characteristics of synthesized PAni-TiO$_2$ nanoparticles were confirmed using FTIR, XRD, PSA, SEM and EDS techniques. Response surface methodology (RSM) based on central composite design (CCD) was used for Design of experiments. Design Expert software optimized 70.59% degradation of 1,2-dichloroethane with catalyst composition [TiO2: PAni] at [2.33:1] and catalyst loading at 0.39 mg/cm², respectively. In this study (1) PAni-TiO$_2$ nanocomposite was successfully immobilized on glass beads, (2) 1,2-dichloroethane was successfully degraded using synthesized PAni-TiO$_2$ nanocomposite under visible light irradiation and (3) the designed and constructed photocatalytic reactor performed well for conducting photocatalytic degradation of 1,2-dichloroethane experiments and (4) for experimental conditions of this work, PAni-TiO$_2$ nanocomposite was more effective than pristine TiO$_2$ under visible light irradiation.

Keywords: Photocatalytic degradation; Photoreactor; 1,2-dichloroethane; PAni-TiO$_2$; Immobilized glass beads; Response surface methodology

1. Introduction

The elimination of chlorinated volatile organic compounds from wastewater has been one of the most important environmental concerns in recent years [1]. 1,2-DCE is one of the most important chlorinated volatile organic compounds and is widely used in industries as solvents, dry cleaners, degreasers, and chemical intermediates in the production of synthetic resins, plastics, and pharmaceuticals [2]. It is a manufactured chemical that is not found naturally in the environment. It is a toxic, volatile, flammable, colorless liquid with a chloroform-like odor [3]. 1,2-DCE has good solubility in water (8.7 g/l), a low sorption coefficient (log k_{oc} = 1.28) and a low Henry coefficient (1.1 × 10^{-3} atm m³/mol), therefore it remains in the water phase in normal environmental conditions [4]. It is determined to be a probable human carcinogen because of the conversion into chloroacetaldehyde, which is considered to have mutagenic properties and has been

* Corresponding author.

listed as a priority pollutant by the U.S. EPA. The maximum contamination level (MCL) for 1,2-DCE in the drinking water is set as 5 µg/L and the maximum contaminant level goal (MCLG) is set as zero by U.S. EPA [3].

A range of methods, including physical, chemical, and biological, has been studied for 1,2-DCE degradation [1,3–7]. Recently, considerable attention has been paid to the advanced oxidation processes (AOPs) due to high chemical stability and low biodegradability of 1,2-DCE [8,9]. Among different AOPs, heterogeneous photocatalysis is a promising non-selective process. Heterogeneous catalysts that are in fact semiconductors such as TiO_2, SnO_2, ZrO_2, ZnO, CdS, and Fe_2O_3, can provide light induced electron-hole pair for redox processes, primarily due to a filled valance band and empty conduction band [10].

TiO_2 is one of the most promising semiconductors used in environmental applications. To initiate redox reactions, the TiO_2 surface is irradiated with sufficient energy to overcome the band gap. Electron-hole pairs are subsequently generated, which may initiate redox reactions on TiO_2 surface. However, low spectral overlap between the absorption spectrum of TiO_2 and the solar emission spectrum limits the commercial potential because of the low photoreaction rates. Further, the photocatalytic activity is limited by the fast charge carrier recombination and low interfacial transfer rates of charge carriers [11].

In order to overcome these drawbacks, some studies have been performed to enhance photocatalytic activity of semiconductors [12]. Polyaniline (PAni) is a kind of conductive polymers and has been widely used to improve electronic conductivity as well as solar energy transfer due to its easy preparation, comparatively low cost and excellent environmental stability. In recent years, PAni polymers have been used to improve the photocatalytic activity of TiO_2 in UV and visible region [13]. TiO_2 is an n-type semiconductor and PAni is a p-type conducting polymer, the combination of which results in reducing band gap energy which results in sensitizing TiO_2 under UV and visible light irradiation and hindering recombination [14]. PAni-TiO_2 nanocomposite was synthesized by different methods including ultrasonic irradiation [15], sol-gel technique [16], template-free method [17], in-situ deposition oxidative polymerization [18] and hydrothermal method [19].

For many years laboratory scale photocatalytic experiments have been carried out using suspended catalyst which is also known as slurry in a batch reactor [20]. However, the need for an expensive and time consuming separation step to retrieve the catalyst and limited penetration depth of the light into the slurry lead to serious problems [21]. Mass transfer limitation and limited specific surface area are problems of this system but a proper reactor design can reduce these drawbacks [22,23].

The immobilization of the catalyst on inert support surfaces has been recently used in order to eliminate the costly phase separation processes [24]. Sol-gel methods including dip coating and spin coating, heat attachment method, chemical vapor deposition (CVD), Electrophoretic deposition and sputter coating have been proposed to prepare immobilized catalysts [25]. Various supports were used including glass, silica gel, metal, ceramics, polymer, fibers, zeolite, alumina clays, activated carbon, cellulose and reactor walls. Glass can

sustain a high calcination temperature and is highly transparent. A number of glass materials are commonly utilized in the photodegradation of polluted water, such as glass plates, glass beads, glass tube, glass rings and walls of reactor [25].

Photocatalytic processes are complicated, because many independent influential parameters such as initial pollutant concentration, catalyst loading, pH, residence time and dissolved oxygen can affect degradation efficiency as the response of the system [26]. Response surface methodology (RSM) establishes a regression mathematical relationship between independent and response parameters for seeking the optimum conditions of a complicated multivariable system with the lowest number of tests [27]. RSM has been successfully applied to various processes to achieve optimization using experimental designs, including photocatalytic degradation of pollutants using immobilized catalysts [28].

To the best of our knowledge, there is no report on the use of PAni-TiO_2 nanoparticles as a photocatalyst for the photocatalytic degradation of 1,2-DCE. The aim of the present study was to investigate the performance of synthesized PAni-TiO_2 nanocomposite for photocatalytic degradation of 1,2-DCE. PAni-TiO_2 nanocomposite was synthesized and immobilized on glass beads. The characteristics of synthesized nanoparticles were confirmed using FTIR, XRD, PSA, SEM and EDS techniques. A photocatalytic reactor in pilot scale was designed and constructed for photocatalytic degradation 1,2-DCE. Two influential parameters of catalyst composition [TiO_2: PAni] and catalyst loading (mg/cm^2) were considered as independent parameters. 1,2-DCE degradation was selected as a response parameter. Response surface methodology based on central composite design was used for Design of experiments. Using the RSM technique, a regression equation was presented to predict the 1,2-DCE degradation. Based on the proposed model, the best values of independent parameters for achieving the highest 1,2-DCE degradation were determined.

2. Material and methods

2.1. Chemicals

All chemicals used in this work were of analytical reagent grade. 1,2-DCE ($C_2H_4Cl_2$, ACS reagent ≥99%, Merck) was used as the target pollutant, n-Hexane ($CH_3 (CH_2)_4CH_3$, HPLC grade, ≥95%, VWR) was used as a solvent to extract 1,2-DCE from aqueous phase samples. TiO_2 nanoparticles (anatase, average crystal size, 20 nm, US Nano) were used to synthesize PAni-TiO_2 nanocomposite, ammonium peroxodesulfate (APS, $(NH_4)_2S_2O_8$) was supplied by Fluka. All other reagents including hydrochloric acid fuming 37% (HCl), Hydrofluoric acid (HF), Aniline, diethyl ether, and ethanol were supplied by Merck (Germany) with analytical grade. Deionized water was used for solution preparation throughout this research.

2.2. Synthesis of PAni-TiO_2 nanocomposite

PAni-TiO_2 nanocomposite was synthesized using in-situ deposition oxidative polymerization method as following: 3.1 g of TiO_2 nanoparticles were dispersed into 90 mL of 1 molar HCl 37% solution containing 1 mL aniline under ultrasonic vibration inside an ice-water bath for 1 h to

reduce the aggregation of TiO_2 nanoparticles. The solution was deoxygenated by flow of nitrogen into the three-neck-round-bottom flask. Then, 2.5 g of APS was dissolved into 100 mL of 1 molar HCl solution. This solution was added dropwise into the solution containing aniline. This mixture was allowed to be polymerized in an ice-water bath under magnetic stirring for 5 h. After that, the prepared mixture was washed and filtered with deionized water, 50 ml of ethanol and 30 ml of ether. After that, the solution was dried at 80°C for 8 h to obtain the PAni-TiO_2 nanocomposite. Flowchart of synthesis of PAni-TiO_2 is shown in Fig. 1 [18,29].

2.3. Immobilization of PAni-TiO_2 nanocomposite

Immobilization of the PAni-TiO_2 nanocomposite on glass beads was carried out by a modified dip coating and heat attachment method. Glass beads with 10 mm diameter were selected as packing material and etched with hydrofluoric acid (HF) 5% for 24 h and washed with deionized water for making a rough surface and were weighted precisely before immobilization. Five different slurry solutions of PAni-TiO_2 with different catalyst compositions were prepared. Each solution contained 3.1 g of PAni-TiO_2 nanocomposite in 200 ml deionized water and was continuously mixed for 24 h. After that, glass beads were immersed in the slurry for 30 min and then removed from the solution and placed in an oven for 1 h at 80°C for drying and then heat-treated using a programmable furnace. Finally, the furnace was allowed to cool down to room temperature. This heat attachment method causes partial sintering of the particles and adhesion of PAni-TiO_2 particles to the glass beads without the need for binders. The cooling down period took approximately 12 h. After that, immobilized glass beads were washed with deionized water to remove unattached photocatalyst particles. Then, the beads were weighted again. The difference between weight of uncoated and coated glass beads is the weight which was immobilized on glass beads. Coating process was repeated several times until certain catalyst loading (i.e.: 0.1, 0.2, 0.3, 0.4 and 0.5 mg/cm²) was reached. After completing

the immobilization, glass beads were removed, mixed and put back in the slurry again to prevent the occurrence of uncoated regions. Flowchart of PAni-TiO_2 immobilization on glass beads is shown in Fig. 2.

2.4. Characterization of PAni-TiO_2 nanocomposite

In this study, different methods of characterization including FTIR, XRD, PSA, SEM and EDS were used to describe the characteristics of synthesized PAni-TiO_2 nanoparticles. X-ray diffraction (XRD) patterns were used to determine the structural characteristics and crystalline phases of nanoparticles using a scattering detector Bruker D8 Advance (Billerica, Massachusetts) at a voltage of 40 kV and 45 mA using radiation CuKα (λ = 1.5406 Å). The XRD pattern data were collected for the 2θ values between 10° and 90° and a scanning rate of 0.02°/s. The Fourier-transform infrared spectra were recorded by using an FTIR spectrometer (spectrum RXI, PerkinElmer). Immobilized PAni-TiO_2 nanoparticles were coated with gold, using a Desk Sputter Coater (Dsr1 Nanostructural coating) and observed via scanning electron microscope (SEM) and EDS (TESCAN Vega 3). Particle size analysis (PSA) was conducted to determine the size distribution of nanoparticles using the HORIBA, DLS Version LB-550.

2.5. Apparatus

A photocatalytic reactor in pilot scale was designed and constructed for photocatalytic degradation of 1,2-DCE. Three cylindrical photocatalytic reactors were connected to each other in series by connecting polyethylene tubes and were mounted on the geometric center of three aluminum collectors (15 cm in diameter, with an axial distance of 20 cm from each other) to reflect radiation of light back into the reactors. Each reactor consists of three concentric cylinders and a central lamp which enables the reactor to perform either visible or UV tests by replacing the lamp. A cylindrical quartz tube surrounded the lamp, a cylindrical Pyrex tube surrounded
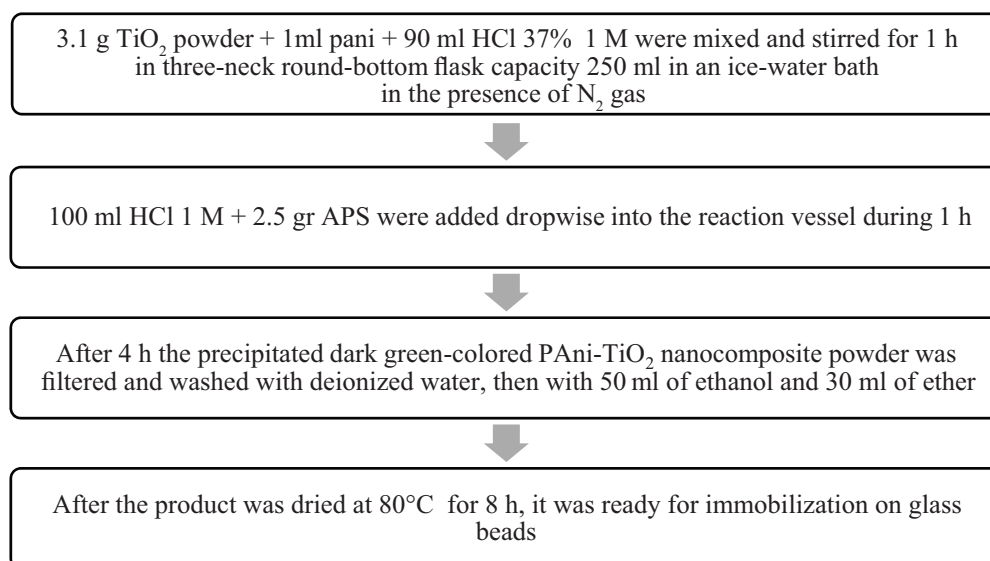

3.1 g TiO_2 powder + 1ml pani + 90 ml HCl 37% 1 M were mixed and stirred for 1 h in three-neck round-bottom flask capacity 250 ml in an ice-water bath in the presence of N_2 gas

⬇

100 ml HCl 1 M + 2.5 gr APS were added dropwise into the reaction vessel during 1 h

⬇

After 4 h the precipitated dark green-colored PAni-TiO_2 nanocomposite powder was filtered and washed with deionized water, then with 50 ml of ethanol and 30 ml of ether

⬇

After the product was dried at 80°C for 8 h, it was ready for immobilization on glass beads

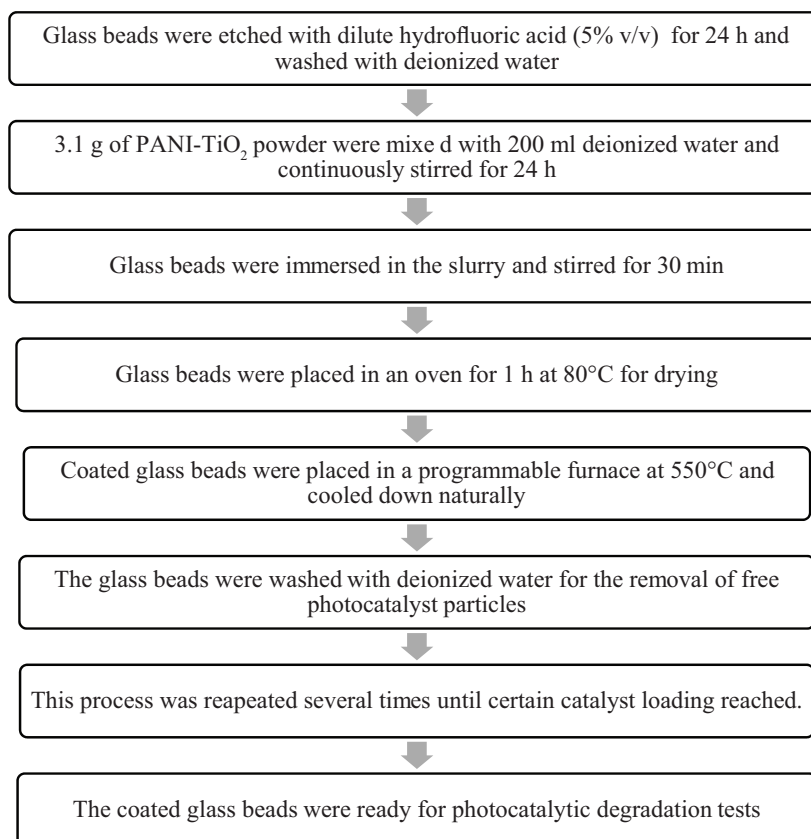Fig. 1. Flowchart of synthesis of PAni-TiO_2 nanocomposite.

Fig. 2. Flowchart of PAni-TiO$_2$ immobilization on glass beads.

the quartz tube for photocatalytic reactions and a Pyrex cylindrical tube surrounded the reaction tube for controlling temperature of the reaction under 15°C through the process by circulation of cooling water to prevent evaporation of 1,2-DCE. Other parts of the photoreactor are shown in Fig. 3.

2.6. Design of experiments

In this research, catalyst composition and catalyst loading were considered as independent parameters. Ranges of these parameters were determined based on literature and preliminary experiments. The removal efficiency of 1,2-DCE was considered as the response parameter. Central composite design (CCD) based on response surface method (RSM) was selected for designing the experiments. Total number of experiments was calculated as:

$$N = 2^k + 2_k + C_0 = 2^2 + 2 \times 2 + 3 = 11 \tag{1}$$

where N is the total number of experiments required, k is the number of parameters, $2k$ is axial runs and C_0 is the center point runs. Design of experiments and results are shown in Table 1.

2.7. Response surface methodology

In this research, response surface method (RSM) based on central composite design (CCD) was applied for design of experiments. RSM presents a multivariable regression

equation to predict the response parameter using the least amount of data. The fitted equation can be a polynomial with a maximum degree of two in the following form:

$$Y_{\text{pred}} = \beta_0 + \sum_{i=1}^{k} \beta_i x_i + \sum_{i=1}^{k} \beta_{ii} x_i^2 + \sum_{i \langle j}^{k} \beta_{ij} x_i x_j \tag{2}$$

where Y_{pred} is predicted value of the response parameter; β_0 is constant coefficient; β_i is linear effect of parameter x_i; β_{ii} is the second order effect of parameter x_i; and β_{ij} is the interaction linear effect of parameter x_i and x_j. The statistical significance of each β coefficient is investigated using the analysis of variance (ANOVA). If the relationship between independent parameters and the response parameter is linear, β_{ii} and β_{ij} will not be significant and must be equal to zero [30]. The results were analyzed using analysis of variance (ANOVA) by Design expert (trial version 10.0.6.0, Stat-Ease Inc.) software.

2.8. Photocatalytic degradation of 1,2-DCE

All tests were carried out at radiation of a 150 W xenon lamp except for blank and adsorption tests, Wastewater flow of 40 L/h, aeration flow of 2 L/min, initial concentration of 200 mg/l and pH of 7. HCl and NaOH (1 M) were used for pH adjustment. Before starting the main experiments, blank, adsorption and photolysis tests were carried out. The blank test was carried out with uncoated glass beads and without
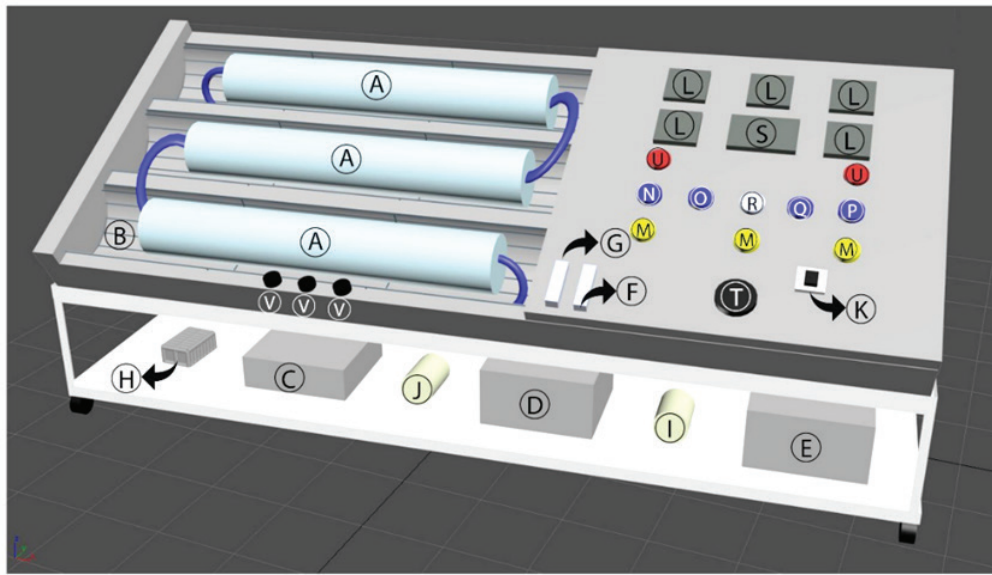
Fig. 3. Schematic of the photo-reactor designed and constructed for photocatalytic degradation of 1,2-DCE: (A) cylindrical photocatalytic reactors, (B) aluminum collectors, (C) Wastewater tank, (D) Water tank, (E) Temperature adjusting tank, (F) wastewater flow meter, (G) air flow meter, (H) Aeration pump, (I) water pump, (J) wastewater pump, (k) power switch, (L) digital temperature controller display, on/off switches for (M) lamps, (N) wastewater pump, (O) water pump, (P) mixer, (Q) water circulation between submersible pumps, (R) air pump, (S) water level monitoring, (T) controller for heater temperature, (U) on/off switch for heaters, and (V) sampling port for each reactor.

Table 1
Central composite design (CCD) matrix and results for photocatalytic degradation of 1,2-DCE

Range and level						
Factors	Units	$-\alpha$	Low (–1)	Middle (0)	High (+1)	$+\alpha$
Catalyst loading	mg/cm^2	0.1	0.2	0.3	0.4	0.5
Catalyst composition	[TiO$_2$:PAni]	0.3	1.0	1.7	2.4	3.1

Design matrix					
Run	Type	Catalyst loading (mg/cm^2)	Catalyst composition [TiO$_2$:PAni]	Degradation % (actual)	Degradation % (predicted)
1	Factorial	0.4	1	51.231	51.677
2	Factorial	0.2	2.4	65.163	65.276
3	Axial	0.3	3.1	74.501	74.526
4	Center	0.3	1.7	60.432	59.587
5	Factorial	0.4	2.4	71.304	71.421
6	Axial	0.5	1.7	66.239	66.097
7	Factorial	0.2	1	48.528	48.971
8	Axial	0.3	0.3	38.781	38.476
9	Center	0.3	1.7	60.025	59.587
10	Axial	0.1	1.7	57.384	57.246
11	Center	0.3	1.7	58.863	59.587

irradiation to find the amount of 1,2-DCE released to the atmosphere after 2 h as a result of circulation, stirring and volatility of 1,2-DCE. In blank test, two samples were taken for GC-MS analysis from wastewater and cooling water respectively. The adsorption test was carried out with coated glass beads and without irradiation to find the amount of 1,2-DCE adsorbed on the surface of coated glass beads. The photolysis test was carried out to find the amount of 1,2-DCE degraded due to irradiation of xenon lamp for 2 h with uncoated glass beads. For all tests, After 2 h, a sample was

withdrawn to calculate the amount of 1,2-DCE removal using the following equation:

$$1,2 - \text{dichloroethane removal} \% = \frac{C_0 - C_t}{C_0} \times 100 \qquad (3)$$

where C_0 (mg/l) is the initial concentration of 1,2-DCE at $t = 0$ and C_0 (mg/l) is the concentration of 1,2-DCE at time t.

2.9. Comparison of photocatalytic activity of PAni-TiO₂ and pristine TiO₂

For investigating the effect of doping on 1,2-DCE degradation efficiency, the photocatalytic activity, the optimum catalyst (catalyst composition [2.4:1] and catalyst loading 0.4 mg/cm²) was compared with the photocatalytic activity of pristine TiO₂ with catalyst loading (0.4 mg/cm²) under visible light irradiation. The same operational parameters of designed tests were applied (wastewater flow of 40 L/h, aeration flow of 2 L/min, initial concentration of 200 mg/l and pH of 7).

3. Results and discussion

3.1. Characterizations of PAni-TiO₂ nanocomposite

As shown in Fig. 4, for the best PAni-TiO₂ composition [2.4:1] (Fig. 4(f)), the main characteristic peaks of doped PAni are assigned as follows: the band at 3,433 and 2,925 cm⁻¹ can be attributed to non-hydrogen bonded N–H stretching vibration and hydrogen-bonded N–H bond between amine and imine sites; C=N and C=C stretching modes for the quinonoid and benzenoid units occur at 1,563 and 1,477 cm⁻¹, the bands at 1,295 and 1,242 cm⁻¹ have been attributed to the C–N stretching mode for benzenoid unit, while the peak at 801 cm⁻¹ is associated with C–C and C–H for benzenoid unit [31] The characteristic peaks of TiO₂ at 1,128 and 506 cm⁻¹ were also found in the spectrum of PAni-TiO₂ nanocomposite. The characteristic peaks from the PAni are seen at 1,295, 1,477 and 1,563 cm⁻¹, corresponding to the stretching modes of C– N and C=N bonds. After titania was introduced, all peaks shifted to higher wavenumbers. The characteristic peak of N–H stretching mode at 3,433 cm⁻¹ of PAni shifted to a lower wavenumber in the PAni-TiO₂ composite, and the hydrogen bond absorption at 2,925 cm⁻¹ is strengthened after TiO₂ was introduced. These findings reveal that the hydrogen bonding in the PAni complex became stronger after complexing with TiO₂. The results also suggest that there is strong interaction between the polyaniline and nanocrystalline TiO₂ [29,32,33].

The particle-size analysis (PSA) was used to achieve a better view of the synthesized PAni-TiO₂ dimensions for the best PAni-TiO₂ composition [2.4:1]. As shown in Fig. 5, mean diameter of particles was 33.5 nanometer. Based on this analysis, it may be argued that during the synthesis, nano-sized particles were produced.

The SEM analysis was used for a better view of the nanoparticles (Fig. 6). Comparison of Fig. 6(a) and Fig. (b) showed that PAni-TiO₂ nanoparticles were successfully immobilized on the surface of glass beads. EDS analysis was used to prove the presence of TiO₂ and PAni (C_6H_7N) on the surface of the samples.
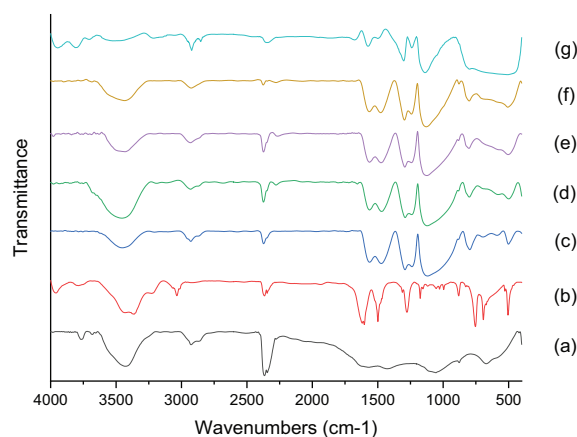

Fig. 4. FT-IR spectra of (a) pure TiO₂, (b) pure PAni, (c) PAni:TiO₂ [1:0.3], (d) PAni:TiO₂ [1:1], (e) PAni:TiO₂ [1:1.7], (f) PAni:TiO₂ [1:2.4], and (g) PAni:TiO₂ [1:3.1].
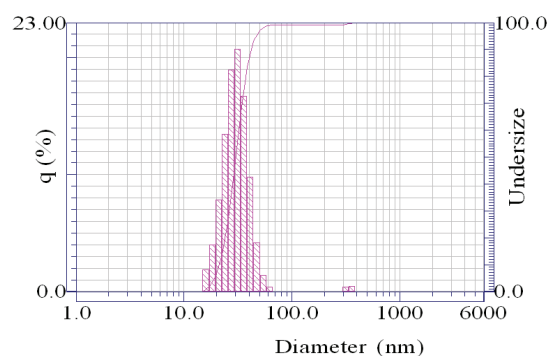

Fig. 5. PSA pattern of PAni-TiO₂.

Fig. 7(a) illustrates EDS spectra of unimmobilized glass beads and Fig. 7(b) illustrates EDS spectra of immobilized glass beads. Based on the results, the peaks of the Ti, O, C and N elements were observed in the sample, and the intensity of each peak was proportional to the weight percentage of atoms.

The X-ray diffraction pattern of PAni-TiO₂ with different compositions is presented in Fig. 8. For the best PAni-TiO₂ composition [2.4:1], the anatase TiO₂ had 2θ values at 25.27°, 37.78°, 48.07°, 54°, 55.11°, and 63°. Therefore, the peaks of 2θ at 10.3°, 14.0°, 15.7°, 16.9°, and 27.4° of PAni disappeared and a peak at 20.8 became weaker. The results suggest that the addition of nanocrystalline TiO₂ hampers the crystallization of the PAni molecular chain and the deposition of PAni on the surface of TiO₂ has no effect on the crystallinity of TiO₂ nanoparticles. Therefore, the polymorph of TiO₂ in the PAni-TiO₂ nanocomposite is still in the anatase form. This is because when the deposited polyaniline is absorbed onto the surface of the nano-TiO₂ particle, the molecular chain of absorbed polyaniline is tethered and the degree of crystallinity decreases [34,35].

3.2. Blank, adsorption and photolysis tests

Result of GC-MS analysis for blank test showed that the amount of 1,2-DCE released to the atmosphere after 2 h
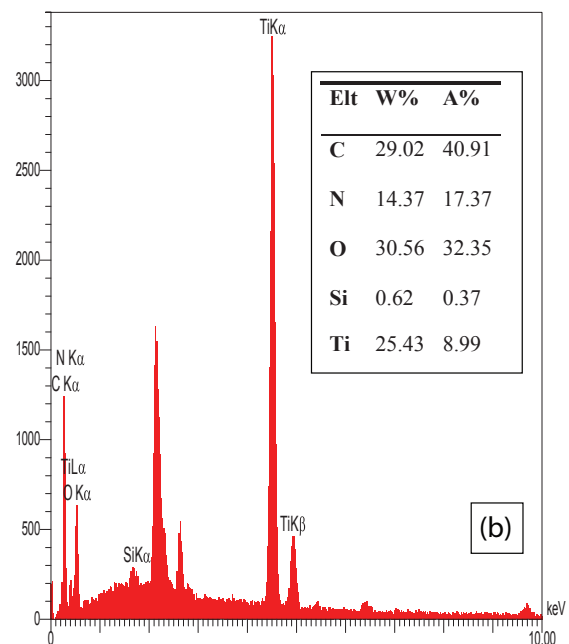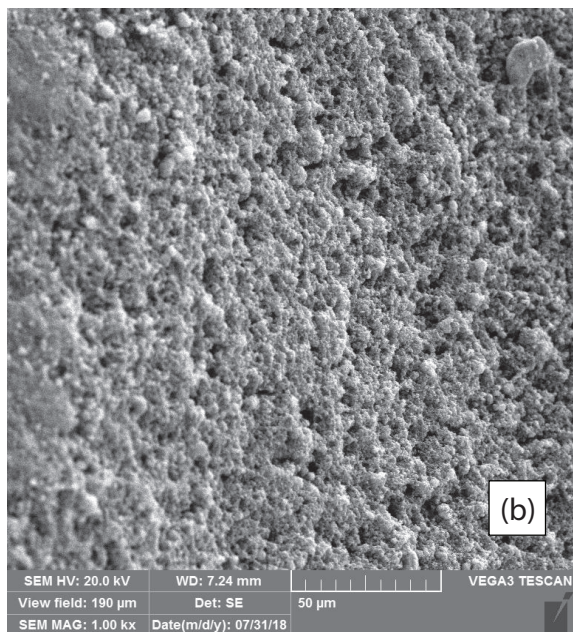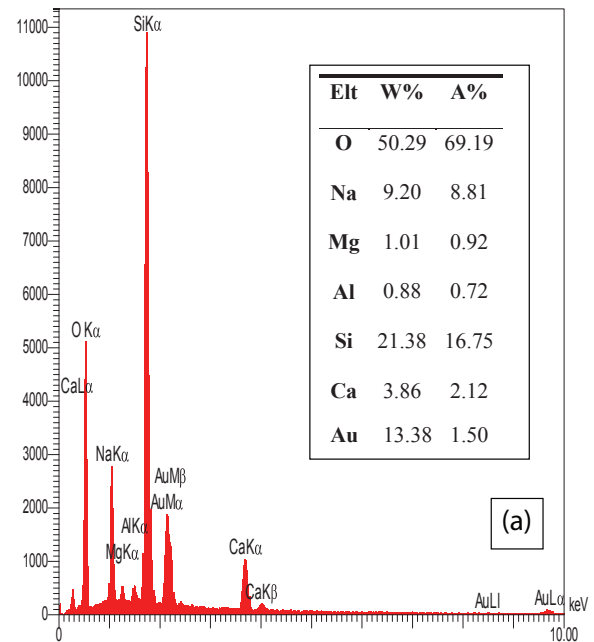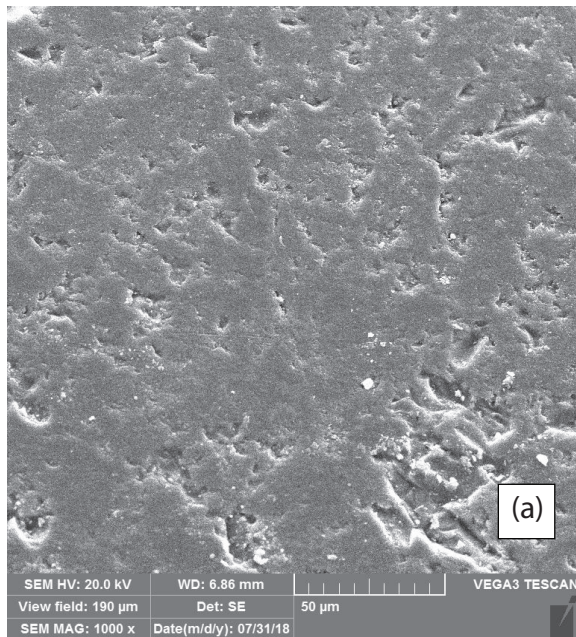
Fig. 6. SEM images for (a) uncoated glass beads and (b) coated glass beads.

Fig. 7. EDS spectra for (a) uncoated glass bead and (b) coated glass bead with PAni:TiO$_2$ (1:2.4).

as a result of circulation, stirring and volatility of 1,2-DCE was 8.36%. Results also showed that the amount of 1,2-DCE entering from wastewater to cooling water was less than 0.1%, which is really negligible and indicates that the reactor was completely sealed. Result of GC-MS analysis for adsorption test showed that the amount of 1,2-DCE adsorbed on the surface coated glass beads was 14.08%. Result of GC-MS analysis for photolysis test showed that the amount of 1,2-DCE degraded due to irradiation of xenon lamp for 2 h with uncoated glass beads was 27.30%. However, the adsorption removal percent of 14.08% is due to the amount of 1,2-DCE released to the atmosphere after 2 h as a result of circulation,

stirring and volatility of 1,2-DCE (8.36%) plus the amount of 1,2-DCE degraded due to adsorption (14.08%–8.36% = 5.72%). Also the photolysis removal percent of 27.30% is due to the amount of 1,2-DCE released to the atmosphere after 2 h as a result of circulation, stirring and volatility of 1,2-DCE (8.36%) plus the amount of 1,2-DCE degraded due to photolysis (27.30%–8.36% = 18.94%). It is evident that mass transfer happens and it should be considered as an experimental error in the analytical results. this results was in agreement

with the results of previous study [5] which reported that (1) without adding any additive and in the absence of radiation (in blank test), the initial concentration of 1,2-DCE in solution decreases by 6%, 12%, and 15% after 2, 4, and 6 h stirring, respectively, and (2) With 24W UV radiation (photolysis), the removal percentages after 2, 4, and 6 h were 15%, 34%, and 48%, respectively.
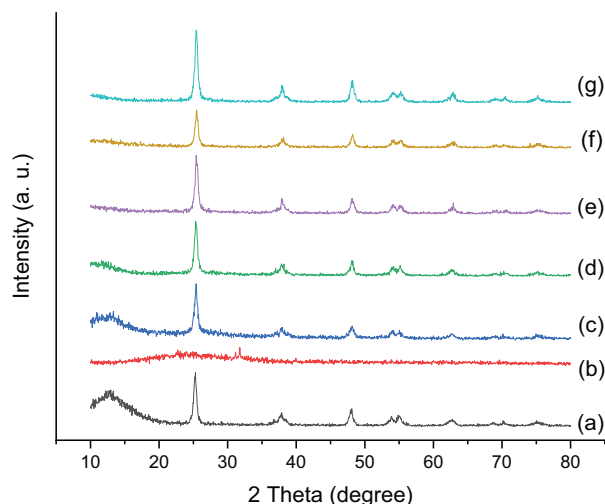

Fig. 8. X-ray diffraction patterns of (a) pure TiO_2, (b) pure PAni, (c) PAni:TiO_2 [1:0.3], (d) PAni:TiO_2 [1:1], (e) PAni:TiO_2 [1:1.7], (f) PAni:TiO_2 [1:2.4], and (g) PAni:TiO_2 [1:3.1].

3.3. Comparison of photocatalytic activity of PAni-TiO₂ and pristine TiO₂

The photocatalytic activity of pristine TiO_2 and PAni-TiO_2 were compared. As shown in Table 2, removal efficiency for PAni-TiO_2 [1:2.4] and pristine TiO_2 was 71.30% and 33.45% respectively which indicates that under visible light irradiation, PAni-TiO_2 has much better performance compared with pristine TiO_2. This is in agreement with the results of previous studies which showed that using pure TiO_2 under UV and solar irradiation had lesser effect than using PAni-TiO_2 on the photocatalytic degradation of organic pollutants [19,29].

3.4. Modeling of photocatalytic degradation using RSM

In order to determine the adequacy of the first-order and second-order model, the normal plots, the residual analysis, the main effects, the contour plot, and analysis of variance (ANOVA) statistics (R^2, adjusted R^2, and lack-of-fit) were examined. As shown in Table 3, the software suggested

Table 2
Effect of PAni-TiO_2 and pristine TiO_2 on the removal efficiency of 1,2-DCE

Catalyst	Pristine TiO_2	Pani-TiO_2 [1:2.4]
Catalyst loading (mg/cm²)	0.39	0.39
C_0 (mg/l)	200	200
C_t (mg/l)	133.08	57.39
Removal efficiency %	33.45	71.30

Table 3
Sequential model fitting for the photocatalytic degradation of 1,2-DCE

Source	Sum of squares	df	Mean square	F- value	Prob > F	Remark
Sequential model sum of squares						
Mean vs. total	38,700.00	1	38,700.00			
Linear vs. mean	1,033.43	2	516.71	128.77	<0.0001	
2FI vs. linear	2.96	1	2.96	0.71	0.4273	
Quadratic vs. 2FI	27.16	2	13.58	34.21	0.0012	Suggested
Cubic vs. quadratic	0.16	2	0.082	0.13	0.8794	Aliased
Residual	1.82	3	0.61			
Total	39,765.53	11	3,615.05			
Lack of fit tests						
Linear	30.78	6	5.13	7.74	0.1188	
2FI	27.82	5	5.56	8.40	0.1098	
Quadratic	0.66	3	0.22	0.33	0.8084	Suggested
Cubic	0.50	1	0.50	0.75	0.4779	Aliased
Pure error	1.33	2	0.66			
Model summary statistics						

Source	Std. Dev.	R^2	Adjusted R^2	Predicted R^2	PRESS	Remark
Linear	2.00	0.9699	0.9623	0.9162	89.30	
2FI	2.04	0.9726	0.9609	0.9204	84.80	
Quadratic	0.63	0.9981	0.9963	0.9930	7.51	Suggested
Cubic	0.78	0.9983	0.9943	0.9385	65.54	Aliased

quadratic model by verifying lack of fit and model summary statistics. The model adequacy was further checked using ANOVA and is depicted in Table 4. The model F-value of 535.78 implies the model is significant. There is only a 0.01% chance that an F-value this large could occur due to noise. Values of "Prob > F" less than 0.0500 indicate model terms are significant. It means all factors, with respect to main, interactions and quadratic terms, are significant. The "lack of fit F-value" of 0.33 implies the lack of fit is not significant relative to the pure error. There is an 80.84% chance that a "lack of fit F-value" this large could occur due to noise. Non-significant lack of fit is good, because we want the model to fit. The "pred R-squared" of 0.9930 is in reasonable agreement with the "Adj R-squared" of 0.9963; i.e. the difference is less than 0.2. "Adeq Precision" measures the signal to noise ratio. In this study, ratio of 77.467 indicates an adequate signal. Therefore, this model can be used to predict the experimental data.

Final equation in terms of actual factorscan be expressed as follows:

$$
\begin{aligned}
1,2 - \text{DCE removal} = \\
+\ & 37.46540 \\
-\ & 30.01680 \times \text{Catalyst loading} \\
+\ & 14.54316 \times \text{Catalyst composition} \\
+\ & 12.28034 \times \text{Catalyst loading} \times \text{catalyst composition} \\
+\ & 52.11265 \times \text{Catalyst loading}^2 \\
-\ & 1.57425 \times \text{Catalyst composition}^2
\end{aligned}
\tag{4}
$$

From the comparison of the graphical representation of actual vs. predicted values, as shown in Fig. 9(a), this model explains perfectly the experimental range studied. The minimal difference between data points and the straight line in Fig. 9(b) explain that studentized residuals follow a normal distribution.

In order to consider the behavior of responses due to the deviation from the center point (X = 0 for each factor while the other factors are kept constant), perturbation plot as a sensitivity analysis was used. Here, the positive effect means that response (Y) increases with enhancement of independent parameter level (X), and the negative effect means that response decreases due to increasing of independent parameter level [9]. As shown in Fig. 10, two independent

parameters had a significant positive effect on the 1,2-DCE removal efficiency. Significant increase in 1,2-DCE removal was observed due to catalyst composition (B) variation. This finding is in accordance with previous studies [18,29,] that
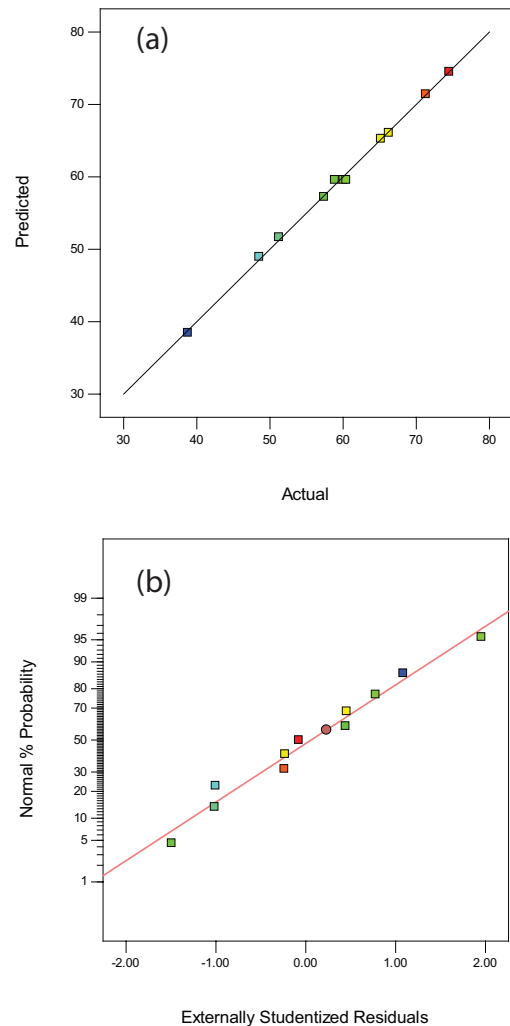

Fig. 9. Plot of (a) actual vs. predicted values of 1,2-DCE removal efficiency and (b) normal probability plots of studentized residuals.

Table 4
ANOVA and lack-of-fit (LOF) test for response surface quadratic model of 1,2-DCE degradation

Source	Sum of squares	df	Mean square	F-value	Prob > F	Remarks
Model	1,063.55	5	212.71	535.78	<0.0001	Significant
A-coating mass	58.75	1	58.75	147.99	<0.0001	
B-catalyst composition [TiO_2:PAni]	974.67	1	974.67	2455.03	<0.0001	
AB	2.96	1	2.96	7.45	0.0414	
A^2	5.24	1	5.24	13.20	0.0150	
B^2	11.49	1	11.49	28.93	0.0030	
Residual	1.99	5	0.40			
Lack of Fit	0.66	3	0.22	0.33	0.8084	Not significant
Pure error	1.33	2	0.66			
Correction total	1065.53	10				

claimed that [PAni: TiO$_2$] with [1:3] composition had the best photocatalytic degradation efficiency. Variation of catalyst loading (A) had a lesser effect on increasing 1,2-DCE removal efficiency. It can be argued that according to [36], when coating mass is thin, the absorption of the light isn't sufficient, therefore, the photocatalyst layer is not as active as its highest possible level. When coating mass increases, light-induced electron-hole pairs created near the photocatalyst-substrate interface which maximizes the rate of photocatalytic degradation. With further increment in the coating mass, light penetration decreases and electron-hole pairs are created far from the photocatalyst-substrate interface, which increases the recombination rate.

Fig. 11(a) illustrates a 3D surface plot of the polynomial which was obtained from Eq. (4) by using the experimental data. It is obvious from contour plot in Fig. 11(b) that when catalyst loading and catalyst composition increase, the degradation efficiency smoothly increases. These findings are in agreement with results of previous works by [29,30].

3.5. Optimization

Optimization was carried on the basis of desirability function in order to find the optimal conditions for the photocatalytic degradation of 1,2-DCE. The criteria for optimization of studied factors in correspondence with degradation percentage are shown in Table 5. Catalyst composition and catalyst loading were assigned as within range with corresponding importance of 3. Higher degradation is usually preferable in photocatalytic degradation tests, so, importance

of 5 was assigned as the maximum goal. The lower limit and upper limit values of all responses are taken from the CCD design levels.

According to Fig. 12, By using all above described settings and boundaries, the software optimized 70.59% degradation of 1,2-DCE with calculating the optimized model factors of catalyst composition [TiO$_2$:PAni] at [2.33:1] and catalyst loading at 0.39, respectively.
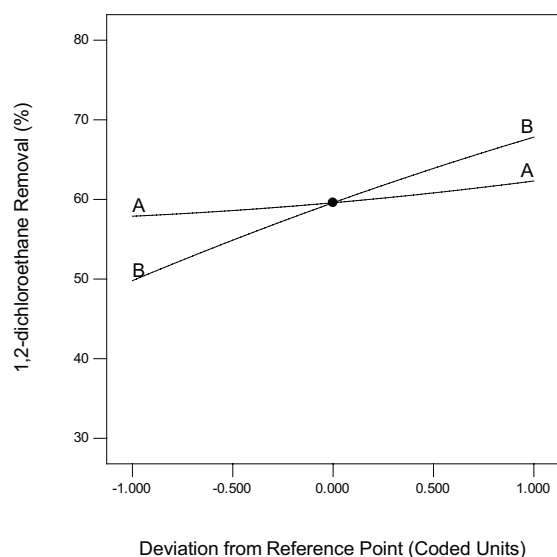

(a)

Fig. 10. Perturbation plot for 1,2-DCE photocatalytic degradation.
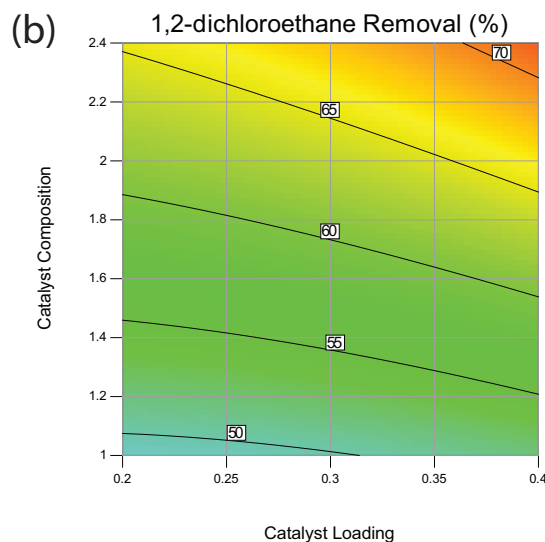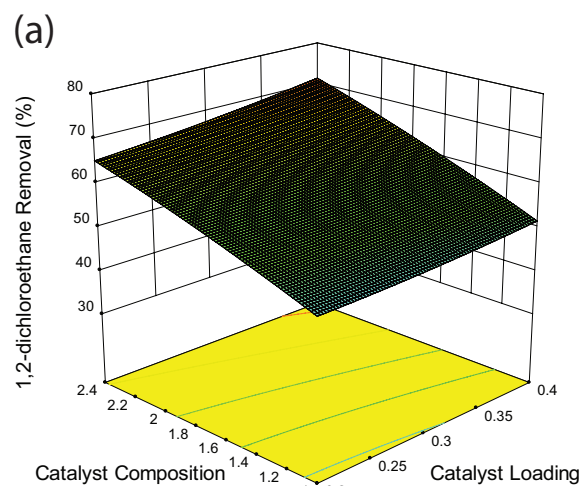
(b)

Fig. 11. (a) 3D response surface and (b) Contour plot for 1,2-DCE photocatalytic degradation.

Table 5
Optimization of the individual responses in order to obtain the overall desirability response

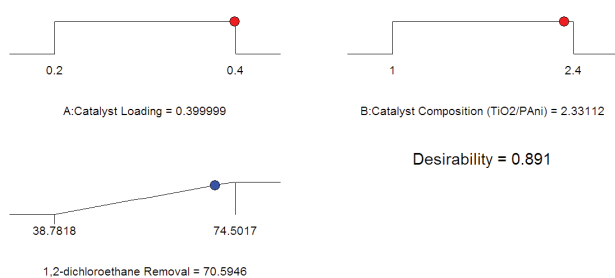| Name	Goal	Lower limit	Upper limit	Lower weight	Upper weight	Importance
Catalyst composition	In range	1	2.4	1	1	3
Catalyst loading	In range	0.2	0.4	1	1	3
1,2-DCE degradation	Maximize	38.7818	74.5017	1	1	5

Fig. 12. Desirability ramp for numerical optimization.

4. Conclusion

The performance of synthesized PAni-TiO$_2$ nanocomposite for photocatalytic degradation of 1,2-DCE in a designed and constructed pilot scale continuous photocatalytic reactor under xenon light irradiation was investigated. The synthesized nanocomposite was immobilized on glass beads by a modified dip coating and heat attachement method. The characteristics of synthesized PAni-TiO$_2$ nanoparticles were confirmed using FTIR, XRD, PSA, SEM and EDS techniques. For optimization of catalyst, two influential parameters of catalyst composition and catalyst loading were considered as independent parameters. 1,2-DCE degradation was selected as the response variable. Based on the results, optimum conditions of catalyst can be reached with catalyst loading of 0.39 mg/cm^2 and catalyst composition of [2.33:1]. In this study (1) PAni-TiO$_2$ nanocomposite was successfully immobilized on glass beads by a modified dip coating and heat attachement method, (2) 1,2-DCE was successfully degraded by using synthesized PAni-TiO$_2$ nanocomposite under visible light irradiation and (3) the designed and constructed packed bed continuous photoreactor performed well for conducting photocatalytic degradation of 1,2-DCE experiments and (4) for experimental conditions of this work, PAni-TiO$_2$ nanocomposite was more effective than pristine TiO$_2$ under visible light irradiation.

Acknowledgement

References

[1] R. Bejankiwar, J.A. Lalman, R. Seth, N. Biswas, Electrochemical degradation of 1, 2-dichloroethane (DCA) in a synthetic groundwater medium using stainless-steel electrodes, Water. Res., 39 (2005) 4715–4724.
[2] M. Vilve, S. Vilhunen, M. Vepsäläinen, T.A. Kurniawan, N. Lehtonen, H. Isomäki, M. Sillanpää, Degradation of 1, 2-dichloroethane from wash water of ion-exchange resin using Fenton's oxidation, Environ. Sci. Pollut. Res.Int., 17 (2010) 875–884.
[3] X. Liu, B.P. Vellanki, B. Batchelor, A. Abdel-Wahab, Degradation of 1, 2-dichloroethane with advanced reduction processes (ARPs): effects of process variables and mechanisms, Chem. Eng. J., 237 (2014) 300–307.
[4] S. De Wildeman, H. Nollet, H. Van Langenhove, W. Verstraete, Reductive biodegradation of 1, 2-dichloroethane by

[5] methanogenic granular sludge in lab-scale UASB reactors, Adv. Environ. Res., 6 (2001) 17–27.
[5] S. Eydivand, M. Nikazar, Degradation of 1,2-Dichloroethane in simulated wastewater solution: a comprehensive study by photocatalysis using TiO$_2$ and ZnO nanoparticles, Chem. Eng. Commun., 202 (2015) 102–111.
[6] Y.H. Lin, W.C. Hung, Y.C. Chen, H. Chu, Photocatalytic degradation of 1, 2-dichloroethane by V/TiO$_2$: the mechanism of photocatalytic reaction and byproduct, Aerosol. Air. Qual. Res., 14 (2014) 280–292.
[7] H. Pham, N. Boon, M. Marzorati, W. Verstraete, Enhanced removal of 1, 2-dichloroethane by anodophilic microbial consortia, Water. Res., 43 (2009) 2936–2946.
[8] A. Stasinakis, Use of selected advanced oxidation processes (AOPs) for wastewater treatment-a mini review, Global. Nest. J., 10 (2008) 376–385.
[9] N. Biglarijoo, S.A. Mirbagheri, M. Ehteshami, S.M. Ghaznavi, Optimization of Fenton process using response surface methodology and analytic hierarchy process for landfill leachate treatment, Process. Saf. Environ., 104 (2016) 150–160.
[10] S. Sarmah, A. Kumar, Photocatalytic activity of polyaniline-TiO$_2$ nanocomposites, Indian. J. Phys., 85 (2011) 713.
[11] S.T. Martin, H. Herrmann, W. Choi, M.R. Hoffmann, Time-resolved microwave conductivity. Part 1. TiO$_2$ photoreactivity and size quantization, J. Chem. Soc. Faraday. T., 90 (1994) 3315–3322.
[12] A. Dawson, P.V. Kamat, Semiconductor metal nanocomposites. Photoinduced fusion and photocatalysis of gold-capped TiO$_2$ (TiO$_2$/gold) nanoparticles, J. Phys. Chem. B., 105 (2001) 960–966.
[13] C.H. Hung, C. Yuan, H.W. Li, Photodegradation of diethyl phthalate with PANi/CNT/TiO$_2$ immobilized on glass plate irradiated with visible light and simulated sunlight effect of synthesized method and pH, J. Hazard. Mater., 322 (2017) 243–253.
[14] M.R. Karim, H.W. Lee, I.W. Cheong, S.M. Park, W. Oh, J.H. Yeum, Conducting polyaniline-titanium dioxide nanocomposites prepared by inverted emulsion polymerization, Polym. Composite., 31 (2010) 83–88.
[15] H. Xia, Q. Wang, Ultrasonic irradiation: a novel approach to prepare conductive polyaniline/nanocrystalline titanium oxide composites, Chem. Mater., 14 (2002) 2158–2165.
[16] D.C. Schnitzler, A.J. Zarbin, Organic/inorganic hybrid materials formed from TiO$_2$ nanoparticles and polyaniline, J. Braz. Chem. Soc., 15 (2004) 378–384.
[17] L. Zhang, M. Wan, Polyaniline/TiO$_2$ composite nanotubes, J. Phys. Chem. B., 107 (2003) 6748–6753.
[18] L. Zhang, P. Liu, Z. Su, Preparation of PANI-TiO$_2$ nanocomposites and their solid-phase photocatalytic degradation, Polym. Degrad. Stab., 91 (2006) 2213–2219.
[19] Y. Lin, D. Li, J. Hu, G. Xiao, J. Wang, W. Li, X. Fu, Highly efficient photocatalytic degradation of organic pollutants by PANI-modified TiO$_2$ composite, J. Phys. Chem. C., 116 (2012) 5764–5772.
[20] D.A. Athanasiou, G.E. Romanos, P. Falaras, Design and optimization of a photocatalytic reactor for water purification combining optical fiber and membrane technologies, Chem. Eng. J., 305 (2016) 92–103.
[21] H. Zeghioud, N. Khellaf, H. Djelal, A. Amrane, M. Bouhelassa, Photocatalytic reactors dedicated to the degradation of hazardous organic pollutants: kinetics, mechanistic aspects, and design-a review, Chem. Eng. Commun., 203 (2016) 1415–1431.
[22] A. Khataee, M. Fathinia, S. Aber, M. Zarei, Optimization of photocatalytic treatment of dye solution on supported TiO$_2$ nanoparticles by central composite design: intermediates identification, J. Hazard. Mater., 181 (2010) 886–897.
[23] P.S. Mukherjee, A.K. Ray, Major challenges in the design of a large-scale photocatalytic reactor for water treatment, Chem. Eng. Technol., 22 (1999) 253–260.
[24] J. Fernández, J. Kiwi, J. Baeza, J. Freer, C. Lizama, H. Mansilla, Orange II photocatalysis on immobilised TiO$_2$: effect of the pH and H$_2$O$_2$, Appl. Catal. B-Environ., 48 (2004) 205–211.
[25] A.Y. Shan, T.I.M. Ghazi, S.A. Rashid, Immobilisation of titanium dioxide onto supporting materials in heterogeneous photocatalysis: a review, Appl. Catal., A., 389 (2010) 1–8.

[26] M. Mohammadi, S. Sabbaghi, Photo-catalytic degradation of 2, 4-DCP wastewater using MWCNT/TiO$_2$ nano-composite activated by UV and solar light, Environ. Nanotechnol. Monit. Manage., 1 (2014) 24–29.

[27] N. Biglarijoo, S.A. Mirbagheri, M. Bagheri, M. Ehteshami, Assessment of effective parameters in landfill leachate treatment and optimization of the process using neural network, genetic algorithm and response surface methodology, Process. Saf. Environ., 106 (2017) 89–103.

[28] A. Khataee, M.N. Pons, O. Zahraa, Photocatalytic degradation of three azo dyes using immobilized TiO$_2$ nanoparticles on glass plates activated by UV light irradiation: influence of dye molecular structure, J. Hazard. Mater., 168 (2009) 451–457.

[29] S. Sabbaghi, M. Mohammadi, H. Ebadi, Photocatalytic degradation of benzene wastewater using PANI-TiO 2 nanocomposite under UV and solar light radiation, J. Environ. Eng., 142 (2015) 05015003.

[30] V.A. Sakkas, M.A. Islam, C. Stalikas, T.A. Albanis, Photocatalytic degradation using design of experiments: a review and example of the Congo red degradation, J. Hazard. Mater., 175 (2010) 33–44.

[31] W. Zheng, M. Angelopoulos, A.J. Epstein, A. MacDiarmid, Experimental evidence for hydrogen bonding in polyaniline: mechanism of aggregate formation and dependency on oxidation state, Macromolecules, 30 (1997) 2953–2955.

[32] Z. Niu, Z. Yang, Z. Hu, Y. Lu, C.C. Han, Polyaniline–silica composite conductive capsules and hollow spheres, Adv. Funct. Mater., 13 (2003) 949–954.

[33] P.R. Somani, R. Marimuthu, U. Mulik, S. Sainkar, D. Amalnerkar, High piezoresistivity and its origin in conducting polyaniline/ TiO$_2$ composites, Synth. Met., 106 (1999) 45–52.

[34] A.G. Yavuz, A. Gök, Preparation of TiO$_2$/PANI composites in the presence of surfactants and investigation of electrical properties, Synth. Met., 157 (2007) 235–242.

[35] T.C. Mo, H.W. Wang, S.Y. Chen, Y.C. Yeh, Synthesis and dielectric properties of polyaniline/titanium dioxide nanocomposites, Ceram. Int., 34 (2008) 1767–1771.

[36] D. Chen, F. Li, A.K. Ray, External and internal mass transfer effect on photocatalytic degradation, Catal. Today., 66 (2001) 475–485.